Applied Physics A (2026) 132:477
https://doi.org/10.1007/s00339-026-09676-y

Applied Physics A
Materials Science & Processing

Asymmetric Au electrode engineering toward high-performance self-powered GaN photodetectors

Sahan Tetik[1] · **Kasif Teker**[1]

Received: 29 January 2026 / Accepted: 24 April 2026
© The Author(s) 2026

Abstract

The demand for high-performance self-powered photodetectors is rapidly increasing due to the growing need for battery-free and maintenance-free sensing in large-scale sustainable electronics and long-lifetime autonomous systems. This study investigates the impact of Au electrode asymmetry on the self-powering mechanism of gallium nitride photodetectors (GaN PDs) under 302 nm and 365 nm UV illumination. The responsivity and detectivity of the GaN PD increased by approximately fifteen times and nine times, respectively, as the Au electrode ratio was changed from 1:2 to 1:20 under 302 nm illumination at 0 V. As a result, excellent responsivity and detectivity values of 8.51 A/W and 2.42×10^{13} Jones were achieved. Furthermore, all our GaN PDs exhibited excellent stability and repeatability under both 302 nm and 365 nm illumination conditions. In summary, GaN photodetectors with asymmetric Au electrode configurations stand out as promising candidates for future UVPD technologies due to their excellent performance and low-cost, straightforward fabrication.

Keywords Asymmetric electrodes · Self-powered photodetectors · GaN PD · Sustainable devices

1 Introduction

In recent years, the energy, robotics, agriculture, space, and healthcare industries have been advancing unlike any time in the past. These advancements both drive and driven by sensors, whose gaining importance with each passing day. Among sensor technologies, photodetectors (PDs) play an increasingly vital role, owing to their fast response times, robustness in challenging environments, and high sensitivity [1, 2]. Ultraviolet photodetectors (UVPDs) stand out due to their solar-blind nature leads to low dark current, and thus enabling enhanced sensitivity compared to conventional PDs [3]. As a result, UVPDs are widely employed in environmental pollution sensors, industrial process monitoring, autonomous navigation and robotics, radiation and nuclear imaging, IoT applications, and flame detection [4–8]. In UVPD applications, wide-bandgap semiconductors are especially employed. These materials are preferred because of their effective absorption of UV photons, intrinsically low dark current enabling solar-blind operation, excellent stability, and their compatibility for self-powered operation due to high built-in potential formation at metal-semiconductor junction [9]. Currently, the most commonly used wide-bandgap semiconductors are GaN [10], SiC [11], ZnO [12], AlGaN [13], β-Ga_2O_3 [14], AlN [15], and diamond [16]. Compared to these semiconductors, GaN is favored owing to its superior electron transport properties and its direct bandgap (E_g = 3.4 eV), for UVPD applications [10].

The performance of the PDs depends on the device structure as important as the choice of semiconductor material. The performance of PDs can be typically enhanced through several routes, such as homojunctions, heterojunctions, and metal nanoparticle coatings. These approaches generally require complex processes such as in-situ doping during Metal-Organic Chemical Vapor Deposition (MOCVD) growth, multi-layer epitaxy, or nanoparticle deposition via physical vapor deposition (PVD) and annealing [17–20]. From the PD configurations, the metal-semiconductor-metal (MSM) architecture has attracted significant attention due to its simple and low-cost fabrication process with suitability for electrode engineering. Thanks to these attributes,

✉ Kasif Teker
kasif.teker@bogazici.edu.tr; kasif.teker@gmail.com

[1] The Advanced Micro- and Nano-Devices Laboratory, Mechanical Engineering Faculty of Engineering, Boğaziçi University, Istanbul, Turkey

Published online: 07 May 2026

MSM structures are an excellent choice for tailor-made self-powered devices. Self-powered devices have gained significant attention in space and defense applications, IoT nodes, and wearable systems due to their ability to operate without an external power source and their low-noise performance [9, 21]. In MSM structures, self-powering mechanism is achieved through the built-in potential differences between electrodes under illumination. In these architectures, self-powered devices are fabricated by two strategies, namely employing asymmetric electrode configuration and selecting different electrode materials [10, 22]. Asymmetric electrode fabrication method is more favorable for self-powered applications than different electrode material method due to simpler fabrication method and the capability to control the built-in electric field by the electrode engineering [23–25]. For instance, it was reported that responsivity of ZnO MSM UVPD improved from 9.3 mA/W to 19.3 mA/W as the size of the smaller electrode reduced by two [25]. A previous study reported a Ga_2O_3 responsivity of 0.149 mA/W, achieved through the use of asymmetric electrode ratio [26]. In another study, the detectivity of an MSM WSe_2 photodetector with an asymmetric electrode configuration reached 9.16×10^{11} Jones [27]. By utilizing an asymmetric ratio of 4, a previous study reported a peak detectivity of 4.07×10^{10} Jones for ZnO MSM UVPD [28]. Therefore, by combining GaN's intrinsically superior material properties with asymmetric electrode engineering in the MSM structures, high performance self-powered devices can be fabricated.

This work systematically investigates, how the photoresponsivity of GaN PDs are varied as a function of electrode ratio (from 1:2 to 1:20) in self-powered mode. Under 302 nm UV illumination and at 0 V bias, the responsivity and detectivity of GaN PD improved from 0.54 A/W to 8.51 A/W and 2.55×10^{12} Jones to 2.42×10^{13} Jones, respectively, by changing the electrode ratio from 1:2 to 1:20. The enhancement was attributed to the built-in potential difference caused by the non-uniform lowering of Schottky barriers at the Au/GaN junctions under illumination. Moreover, all our GaN PD devices exhibited excellent stability and repeatability. Overall, GaN PDs with asymmetric Au electrode ratio emerge as a strong candidate for next-generation self-powered UVPDs due to their high performance with low-cost and simple fabrication.

2 Experimental

The GaN photodetector (GaN PD) was fabricated using a layered structure consisting of Mg-doped GaN (1.0×10^{20} cm^{-3}, 2.5 µm), undoped GaN (2.5 µm), and a sapphire (0001) substrate, from top to bottom. The GaN substrate was diced for device fabrication. The samples were sequentially cleaned with acetone, isopropyl alcohol (IPA), and deionized (DI) water, followed by drying with pressurized nitrogen gas. After the cleaning process, physical mask positioned at the surface of the GaN wafer for formation of asymmetrical Au electrode ratio of (1:20). Then, the wafer was placed into a sputter deposition system and Au electrodes were deposited. The areas of the large and small electrodes were 28.8 mm^2 and 1.44 mm^2, respectively. The gap width and length were 50 µm and 0.8 mm, respectively. Afterwards, the electrode asymmetry ratio ranged from 1:2 to 1:20. Thereby, the size of the large electrode was systematically reduced to 14.4 mm^2 (1:10), 7.2 mm^2 (1:5), and 2.88 mm^2 (1:2) by adjusting the electrode length. Fabrication steps of the GaN PD were shown in Fig. 1. The raw material cost was calculated to be approximately $4.22 for the GaN PD (1:20), consisting of $4.2 for GaN and ~$0.02 for Au. In our market research, a GaN photodiode with an area of 1 mm^2 is commercially sold for approximately $79. In general, the commercial price of photodetectors is typically 5–10 times higher than the raw material and production cost due to packaging, testing, and profit margins. Thus, the calculated device cost in this work supports the claim of low-cost production.

GaN wafer was examined by scanning electron microscopy (SEM, Thermo Scientific Quattro S) and atomic force microscopy (AFM, Ambios Quesant Universal SPM) for morphological analysis and x-ray diffraction (XRD, Bruker D8 Discover) for structural analysis. Optoelectrical measurements were performed using a Keithley 2643B

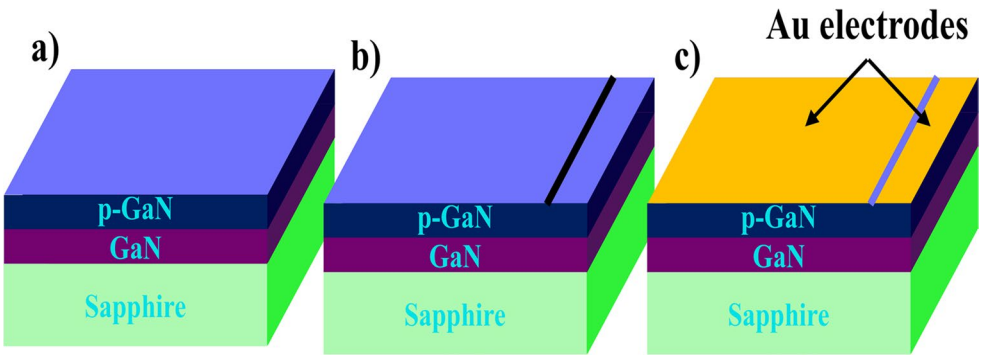

Fig. 1 Fabrication steps of the GaN PD with asymmetrical Au electrodes

Sourcemeter connected to a probe station in a dark environment under UV illumination at 302 and 365 nm with power densities of 1.6 and 1.5 mW/cm², respectively, using a UVP UVLMS-38 UV lamp. Lastly, Tektronix TDS 2024 C was used to measure the rise and decay time of the GaN PD.

3 Results and discussion

First, the morphological analysis of the GaN wafer was conducted through SEM imaging. Figure 2(a) presents a magnified image of the smooth surface of the GaN wafer.

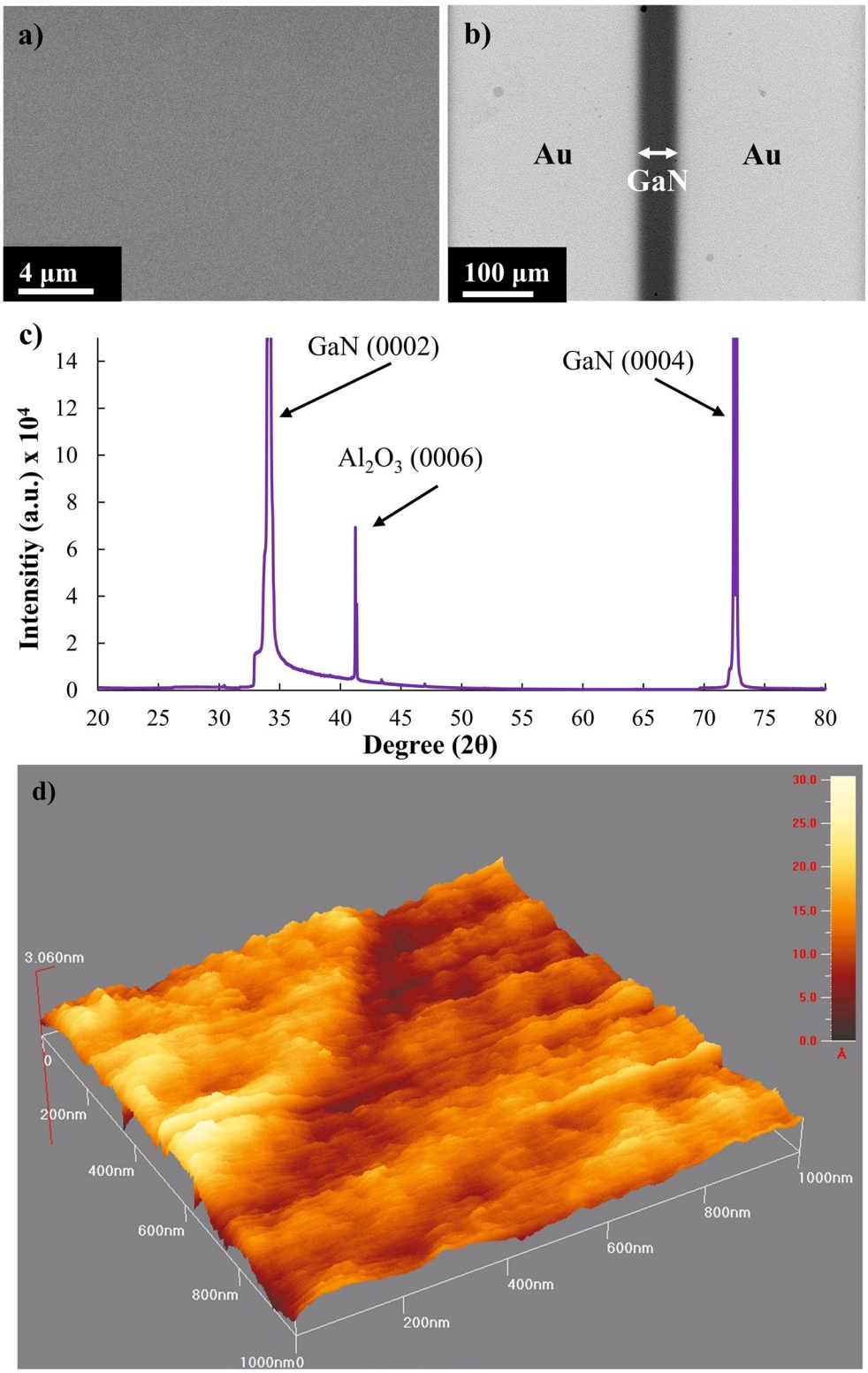

Fig. 2 (**a**) A high magnification SEM image of the GaN surface; (**b**) an SEM image of the GaN photodetector with 50 µm gap; (**c**) XRD pattern of the single crystalline GaN grown on a sapphire substrate; (**d**) Three-dimensional AFM surface image of the GaN wafer (1 µm × 1 µm)

Figure 2(b) shows the fabricated GaN photodetector with asymmetric electrodes and a 50 µm gap width. Figure 2(c) presents the XRD pattern of the GaN wafer, where the diffraction peaks correspond to the hexagonal wurtzite crystal structure, with GaN (0002) and GaN (0004) reflections at 34.58° and 72.85°, respectively. The peak at 41.68° is attributed to the sapphire (0006) plane. Figure 2(d) presents the 3D morphological map of the GaN wafer over a 1 µm × 1 µm area. AFM analysis was performed at three different regions of the surface. The measurements reveal an average roughness (Ra) of 0.29 nm, confirming that the GaN wafer exhibits a highly smooth and uniform surface.

Following the morphological and structural analysis, the optoelectrical measurements were conducted. Figure 3 demonstrates the I-t characteristics of the GaN (1:2) PD under 302 nm and 365 nm UV illumination at 0 V. Moreover, the device showed excellent stability, repeatability, and sharp response under both UV illuminations. The net photocurrent ($I_{ph} = I_{on} - I_{off}$) of the GaN (1:2) PD was measured as 0.35 µA and 0.08 µA under 302 nm and 365 nm lights, respectively. The expression used to evaluate the photon energy-bandgap condition is λ_c (nm)$\geq$1240/E_g (eV), where λ_c and E_g are wavelength and bandgap energy, respectively. Given the bandgap energy of GaN is 3.4 eV [29], the corresponding photon wavelength is 365 nm. Interestingly, the GaN (1:2) PD exhibited more than four times better performance under 302 nm UV illumination compared to its performance under 365 nm UV light. In our earlier studies, we observed a similar finding, where the GaN UVPD exhibited a photocurrent of 650 nA under 302 nm UV illumination, while it was only 130 nA under 365 nm UV illumination [10]. The main reason behind this phenomenon is that when a semiconductor material is exposed to illumination with photon energy exceeding its bandgap, strong optical absorption occurs, resulting in the generation of a large number of electron-hole pairs. Consequently, considerable internal gain may be observed, leading to high photoconductive gain and a significant change in the electrical conductivity under UV illumination [30, 31].

Figure 4 shows the transient characteristics of the GaN PD with asymmetric Au electrode ratios of 1:20, 1:10, 1:5, and 1:2 without external bias under 302 (a) nm and 365 (b) nm. All the GaN PDs exhibited exceptional stability, repeatability, and rapid response under both UV illuminations. Moreover, for each asymmetric Au electrode configuration, the photoresponse measured under 302 nm illumination was significantly higher than that measured under 365 nm illumination, when compared within the same electrode ratio. The net photocurrent of the GaN PD improved from 0.35 µA to 1.53 µA, 2.13 µA, and 5.45 µA by increasing asymmetric Au electrode ratio from 1:2 to 1:5, 1:10, and 1:20, respectively, under 302 nm UV light illumination. Furthermore, a similar trend was observed for the 365 nm UV illumination. In fact, the net photocurrent increased by approximately 4-fold, 12-fold, and 53-fold for 1:5, 1:10, and 1:20 electrode ratios, respectively, compared to the GaN PD with a 1:2 Au electrode ratio. This trend indicates that the enhancement in net photocurrent is closely related to the degree of Au electrode asymmetry, which influences the interfacial electrostatic conditions. Moreover, the transient overshoot observed during the rise phase of the photocurrent, particularly under 302 nm illumination, can be attributed to trap-assisted carrier dynamics in the GaN photodetectors. As the illumination wavelength moves away from the bandgap energy of GaN (~365 nm), higher-energy photons (302 nm) are capable of activating additional excitation pathways, including trap-assisted transitions and surface state involvement. While band-to-band transitions dominate

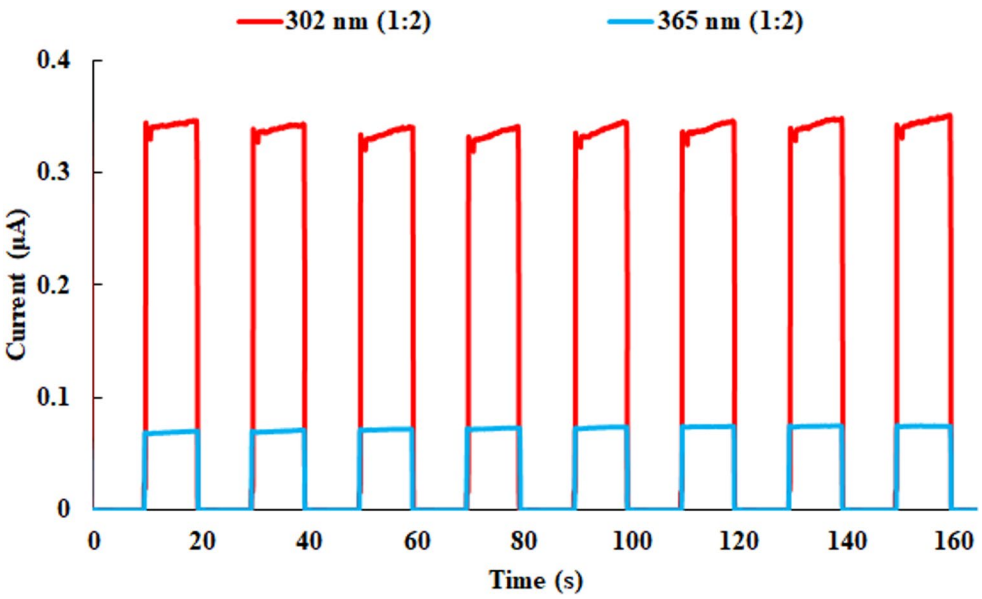

Fig. 3 Photocurrent transient characteristic comparison of the GaN PD with 1:2 Au electrode ratio under 302 nm and 365 nm at zero bias. The GaN PD under 302 nm showed a better performance under 302 nm

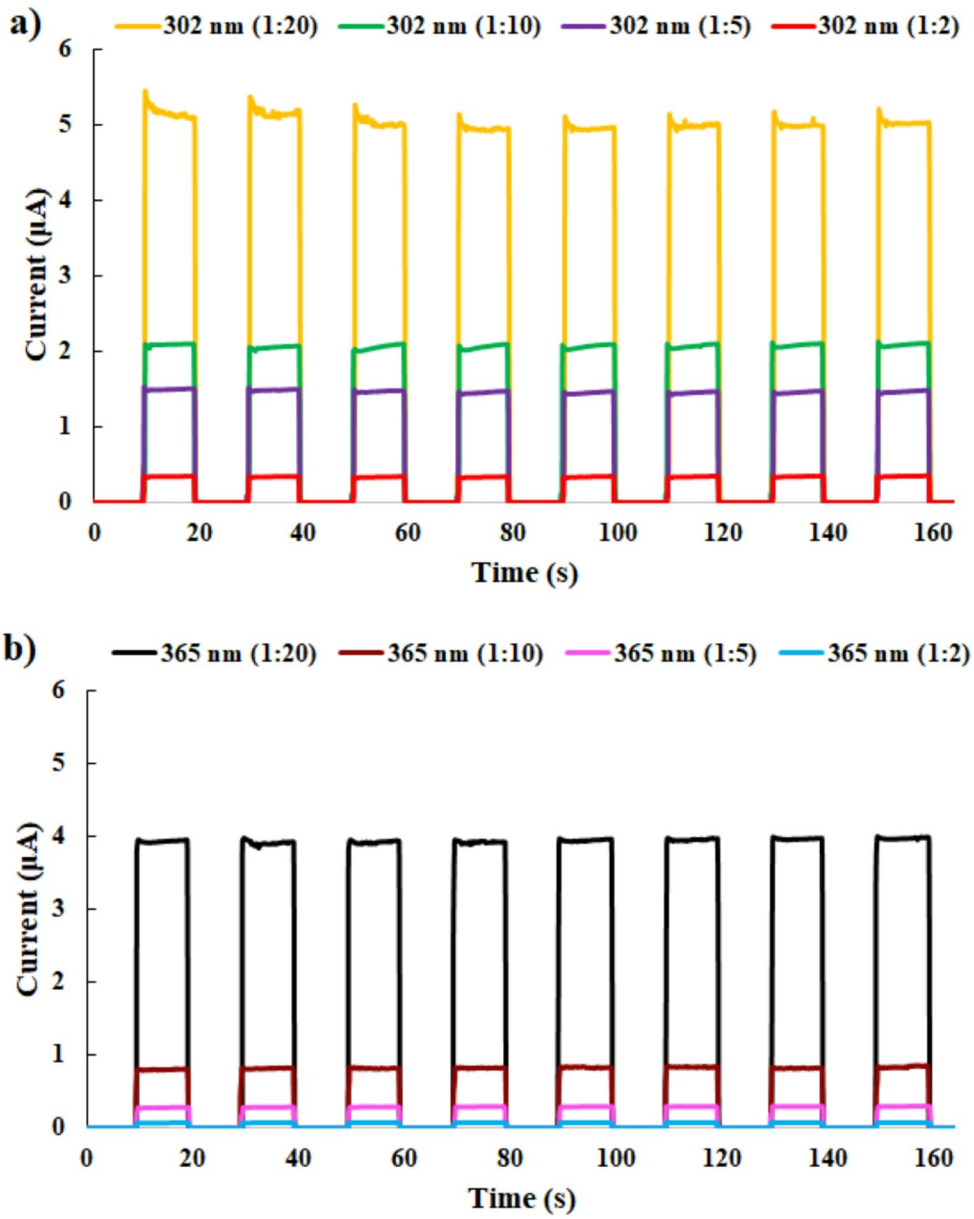

Fig. 4 Current vs. time characteristics of the GaN PDs with Au electrode ratios of 1:20, 1:10, 1:5, and 1:2 measured under self-powered operation (0 V) at wavelengths of 302 nm (**a**) and 365 nm (**b**). The photocurrent markedly increases with increasing asymmetry in the Au electrode ratio. Moreover, all the GaN PDs exhibit excellent stability, repeatability, and fast response under both 302 nm and 365 nm UV illumination

under 365 nm illumination, the excess photon energy at 302 nm promotes carrier trapping at surface and interface states [32–34]. This trapping and subsequent release of carriers causes a temporary buildup of charge, giving rise to a transient current overshoot [35]. Furthermore, as the electrode area increases, the density and probability of surface trap states at the Au/GaN interface also increase [35]. This might be intensified the carrier trapping and release dynamics, resulting in a more pronounced overshoot behavior. Consequently, the overshoot becomes more pronounced in devices with higher electrode asymmetry, particularly in the 1:20 configuration, while it remains negligible in the 1:2 device due to the reduced influence of trap states.

After evaluating the self-powered transient characteristics of the GaN PDs, the I–V measurements were presented in Fig. 5 under 302 nm (a), 365 nm (b), and dark (c) conditions. Under both UV illuminations, the minimum current shifted toward more negative voltage values as the asymmetric electrode ratio changed from 1:2 to 1:20. This shift indicates that the effective built-in potential depends on the electrode ratio under UV illumination. However, under dark conditions, the minimum current was observed at 0 V for all devices, suggesting the absence of a considerable built-in potential gradient. Nevertheless, the dark current at 0 V decreased from 156 pA to 102 pA as the electrode ratio changed from 1:2 to 1:20, which can be attributed to the enlargement of the depletion width.

The substantial improvement of self-powered characteristic by increasing the Au electrode size asymmetry can be attributed to different electrostatic conditions at Au/GaN

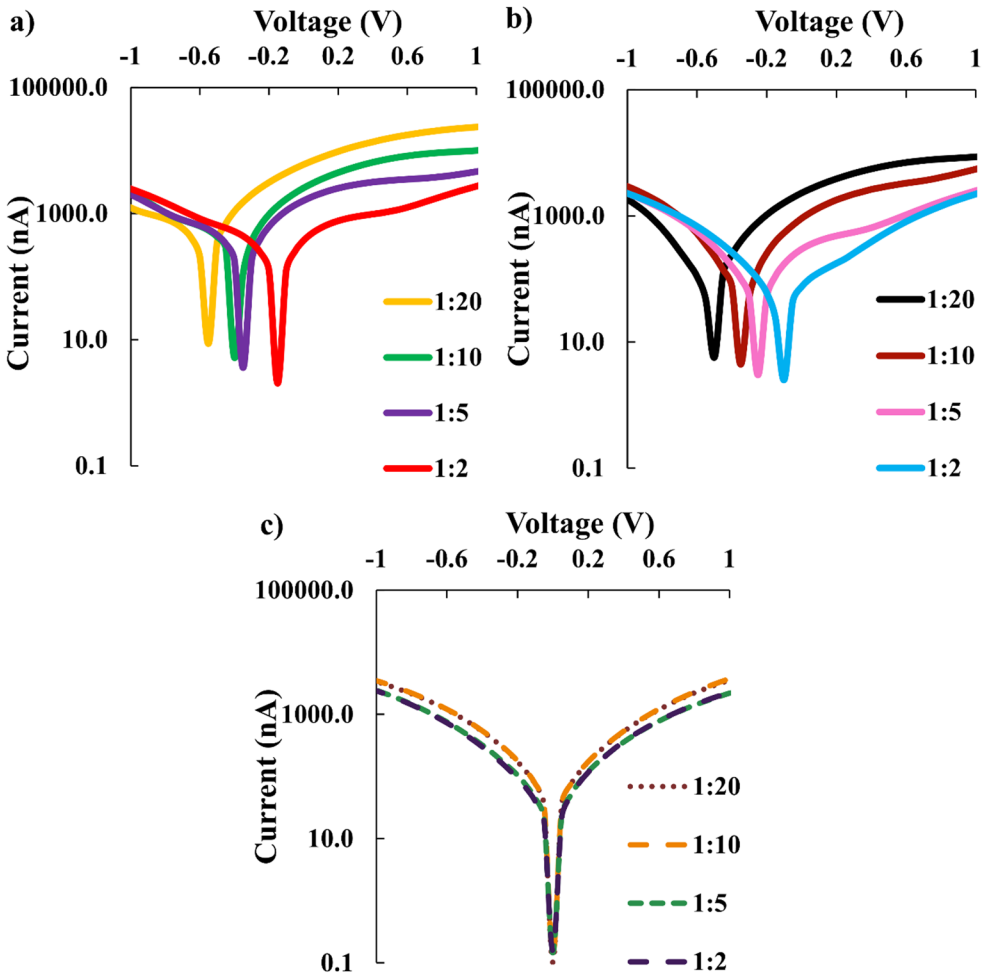

Fig. 5 Current–voltage (I–V) characteristics of the GaN UV photodetectors with different asymmetric electrode ratios (1:2, 1:5, 1:10, and 1:20) measured under (**a**) 302 nm, (**b**) 365 nm illumination, and (**c**) dark conditions. Under UV illumination, the minimum current point shifts toward more negative voltages as the electrode ratio increases, indicating that the effective built-in potential is dependent on the electrode asymmetry

Schottky junction formation. Under dark, both Au/GaN junctions exhibit the same Schottky barrier height, which originates from work function differences between Au and GaN. However, due to the Au electrode size asymmetry, the depletion width of large Au electrode widened more compared to the small Au electrode [23, 24]. In general, for Schottky contacts between p-type semiconductors and metals, the negatively charged ionized acceptors formed on the semiconductor side. As the Au electrode size increases, the larger contact area extends the effective depletion region, thereby increasing the associated negative space charge, and thus altering the local electric field compared more to the smaller electrode [24]. Upon initial stage of UV illumination, electron-hole pairs were generated in the GaN PD. Electrons were repelled from the negatively charged depletion regions, while holes are attracted towards the Au/GaN junction. It was reported in other studies that accumulated photogenerated holes to metal-semiconductor junction can lead to modification of local electrostatic potential and resulting in lowering of built-in potential [24, 25]. Because the junction of large Au electrode and GaN possessed more extensive depletion region, it attracted a higher density of photogenerated holes, leading stronger built-in potential barrier lowering compared to the small Au electrode GaN junction [10, 24, 25]. The asymmetric reduction of Schottky barrier height established a built-in potential gradient from the smaller electrode toward the larger electrode. Consequently, photogenerated electrons drift toward the large Au electrode, while the holes were trapped in depletion region. As the ratio between the large and small Au electrodes increases, the asymmetry in the effective built-in potential becomes more pronounced, strengthening built-in potential gradient. Figure 6 demonstrates the energy band diagram of the GaN with asymmetric Au electrode ratio. Additionally, interface states and surface traps at the Au/GaN junction may capture photogenerated holes, leading to local charge accumulation and additional band bending at the junction [36]. Thus, this can lead to a reduction in the effective Schottky barrier height under UV illumination. Furthermore, due to the higher probability of surface trap formation at the larger electrode compared to the smaller one, the built-in potential reduction becomes more pronounced, which enhances the built-in potential gradient between the smaller and larger electrodes [35].

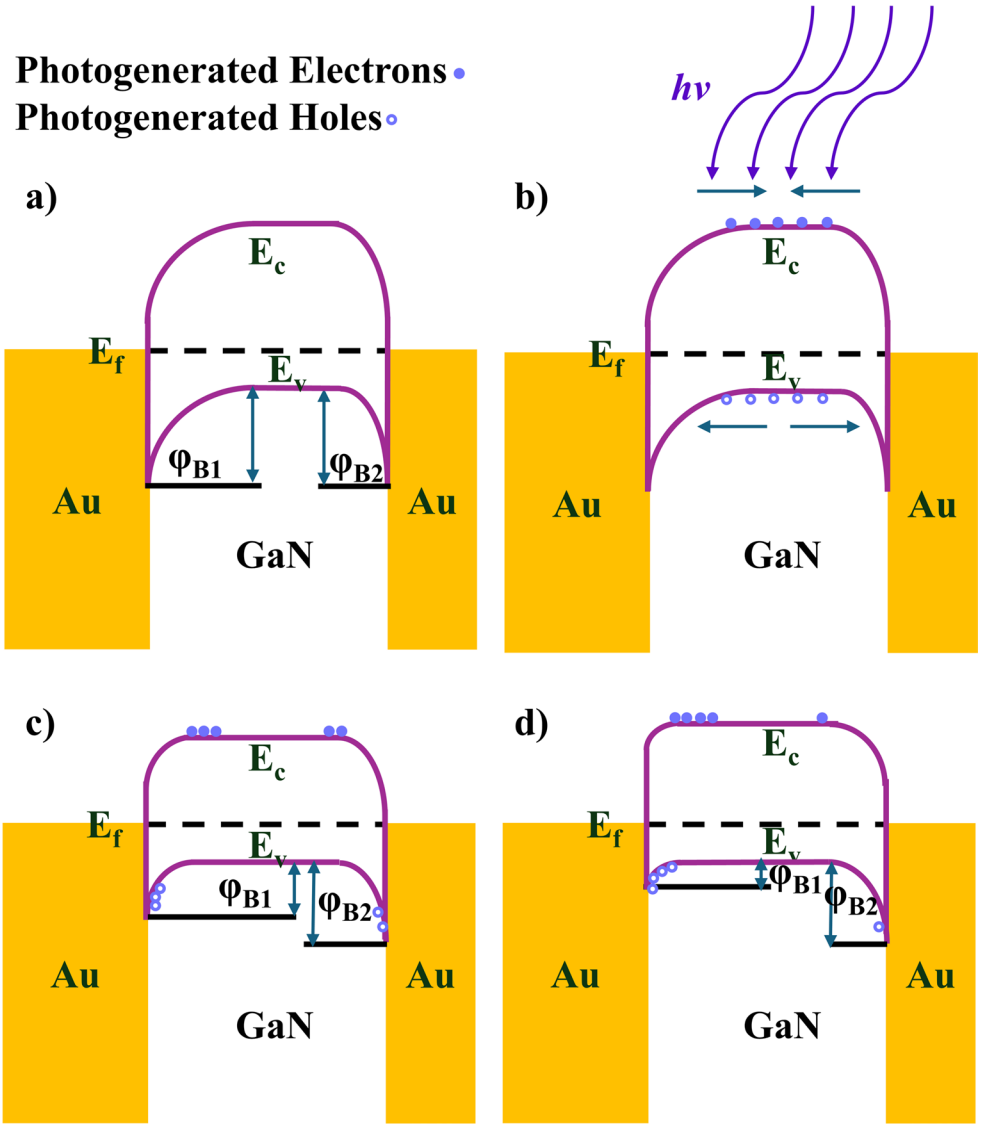

Fig. 6 Schematic energy band diagrams of the asymmetric Au-GaN PD with different Au electrode ratios (**a**) under dark conditions, (**b**) at the initial stage of UV illumination, (**c**) after prolonged UV illumination for the small Au electrode ratio asymmetry, and (**d**) after prolonged UV illumination for large the Au electrode ratio asymmetry. (E_f: Fermi level, E_v: Valence band, E_c: Conduction band, φ_{B1}: Schottky barrier height at the large electrode, and φ_{B2}: Schottky barrier height at the small electrode)

Next, the response speed of the GaN PD (1:20) was evaluated. Figure 7 demonstrates the rise time and decay time characteristics of the GaN PD under 302 nm and 365 nm UV illumination. The rise time (t_r) was defined as the time required for the device current to increase from 10% to 90% of its steady-state value. The GaN PD showed rise times of 43 ms and 84 ms under 302 nm and 365 nm UV light illuminations, respectively. The decay time (t_d) was evaluated as the time interval for the device current to decrease from 90% to 10% of its steady-state dark current. The GaN PD exhibited decay times of 100 ms and 160 ms under 302 nm and 365 UV light exposures, respectively.

After evaluating the optoelectrical and response speed characteristics, the key performance parameters are discussed to evaluate the operational performance of the GaN PDs. Two important performance parameters commonly used to characterize photodetectors are responsivity (R) and specific detectivity (D^*). Responsivity is a key performance parameter, which quantifies the photodetectors efficiency to convert incident light into the electrical signal [10]. Responsivity is calculated by $R = (I_{ph})/(P_\lambda \times A)$, where I_{ph} is net photocurrent, P_λ is the intensity of the incident light, and A stands for effective exposed area. Under 302 nm and 365 nm, responsivity of the GaN PDs gradually improved with increased asymmetrical Au electrode ratio. The responsivity of the GaN PD increased by 4-fold (1:5), 6-fold (1:10), and 16-fold (1:20) compared to the asymmetric Au electrode ratio of 1:2 under 302 nm without using any external voltage source. Furthermore, the responsivity under 365 nm increased from 0.13 A/W to 0.49 A/W, 1.44 A/W, and 6.67 A/W for the asymmetric Au electrode ratios of 1:2, 1:5, 1:10, and 1:20, respectively. Another key performance parameter is specific detectivity ($cm.Hz^{1/2}.W^{-1}$, Jones). Specific detectivity is used to determine the photodetector's

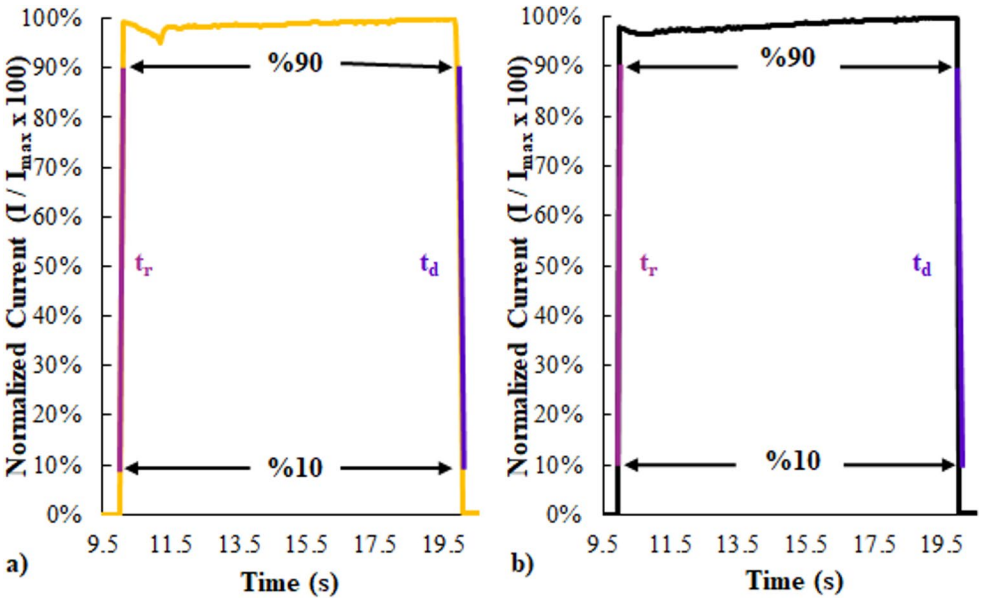

Fig. 7 Rise time (t_r) and decay time (t_d) of the GaN PD under (**a**) 302 nm and (**b**) 365 nm UV illumination

Table 1 Comparison of responsivity and detectivity values of the GaN PDs with asymmetric Au electrode ratios of 1:20, 1:10, 1:5, 1:2 under 302 nm and 365 nm UV lights at 0 V bias. Both, responsivity and detectivity were correspondingly enhanced by increasing the asymmetrical Au electrode ratio

	302 nm		365 nm	
	Responsivity (A/W)	Detectivity (Jones)	Responsivity (A/W)	Detectivity (Jones)
GaN (1:20)	8.51	2.42×10^{13}	6.67	1.82×10^{13}
GaN (1:10)	3.32	1.48×10^{13}	1.44	1.05×10^{13}
GaN (1:5)	2.39	8.34×10^{12}	0.49	3.19×10^{12}
GaN (1:2)	0.54	2.55×10^{12}	0.13	1.04×10^{12}

sensitivity for very weak optical signals in the presence of noise [10]. Specific detectivity (D^*) is obtained from $D^* = (R \times A^{1/2})/(2 \times q \times I_{off})^{1/2}$, where R refers to the responsivity, A corresponds to the effective exposed area, q is the electronic charge, and I_{off} represents the dark current. Similarly, under both 302 nm and 365 nm UV illumination, the specific detectivity of the devices showed significant enhancement as the Au electrode asymmetry increased. The specific detectivity of GaN PD rose by one order of magnitude (from 2.55×10^{12} Jones to 2.42×10^{13} Jones) as the asymmetric Au electrode ratio was 1:20 compared to Au electrode ratio of 1:2 under 302 nm UV light. Moreover, GaN PD's specific detectivity increased from 1.04×10^{12} (1:2) Jones to 3.19×10^{12} Jones (1:5), 1.05×10^{13} Jones (1:10), and 1.82×10^{13} Jones (1:20) under 365 nm without using any external bias voltage. Table 1 presents a comprehensive analysis of the responsivity and specific detectivity values of all the GaN PDs under both 302 nm and 365 nm UV illumination at 0 V. Under both illumination conditions, the GaN photodetector (1:20) exhibited excellent responsivity and specific detectivity.

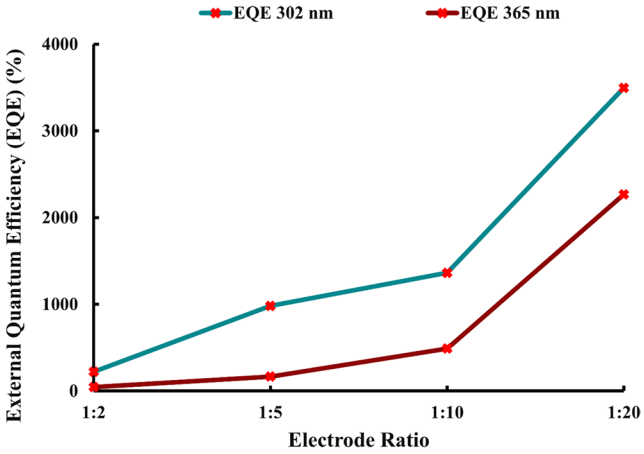

Fig. 8 External quantum efficiency (EQE) of the GaN UV photodetectors as a function of electrode ratio under 302 nm and 365 nm illumination. The EQE values increase significantly with increasing electrode asymmetry, rising from 222% (302 nm) and 44% (365 nm) at a 1:2 ratio to 3494% (302 nm) and 2266% (365 nm) at a 1:20 ratio

After evaluating the performance parameters, the external quantum efficiency (EQE) (%) was calculated using EQE (%) = (R x h x c)/(q x λ) x 100, where R is responsivity, h is Planck constant, c is the speed of light, q is the electronic charge, and λ is the incident wavelength. The EQE values increased significantly from 222% (302 nm) and 44% (365 nm) to 3494% (302 nm) and 2266% (365 nm), respectively, by changing electrode ratio from 1:2 to 1:20. This remarkably high EQE indicates the presence of an internal gain mechanism under zero-bias conditions. Under UV exposure, the asymmetric electrode configuration generates a built-in potential gradient, enabling efficient separation and drift of extrinsic carriers even without an external bias. Figure 8 shows the external quantum efficiency (EQE)

Table 2 Comparison of responsivity, detectivity, rise time, and decay time of the proposed GaN PD with other self-powered photodetectors reported in the literature

Material/Structure	Wavelength (nm)	Responsivity (A/W)	Detectivity (Jones)	Rise Time (ms)	Decay Time (ms)	Ref.
β-Ga_2O_3/GaN	355	2.6	2.3×10^{7}	-	- -	[37]
Nanoporous Ga_2O_3/GaN	254	0.04	2.7×10^{11}	-		[38]
GaN/Ga_2O_3	365	0.054	1.23×10^{11}	100	80	[40]
GaN-UVPD-Au20s	302	0.65	6.51×10^{12}	-	-	[10]
n-GaN/p-ZnTe with Au NPs	325	0.149	2.33×10^{12}	-	-	[39]
AgNWs@ZnO: Ga/MgO/GaN	375	0.262	1.97×10^{12}	-	-	[41]
Sb_2S_3 Thin-Film PD	530	3.41	2.84×10^{13}	-	-	[42]
Au NPs@4H-SiC MSM	254	0.30	7×10^{11}	-	-	[43]
GaN PD (1:20)	302	8.51	2.42×10^{13}	43	100	This Work
GaN PD (1:20)	365	6.67	1.82×10^{13}	84	160	This Work

(%) of the GaN UV photodetectors as a function of the electrode ratio under 302 nm and 365 nm illumination.

Table 2 presents a performance comparison between our GaN photodetector (1:20) and other reported studies operating under zero-bias conditions. For improving the photoperformance of UVPDs at self-powering operation mode, various approaches have been proposed including metal nanoparticles (NPs) mediated plasmonic enhancement and heterostructure architectures. For instance, it was reported that a β-Ga_2O_3/GaN heterostructure achieved an excellent responsivity of 2.6 A/W under 355 nm UV illumination [37]. In a similar study, nanoporous Ga_2O_3/GaN exhibited a decent detectivity of 2.7×10^{11} Jones under 254 nm UV light [38]. In another study, n-GaN/p-ZnTe covered with Au NPs showed very good responsivity and detectivity values of 0.149 A/W and 2.33×10^{12} Jones, respectively [39]. Compared with other reported studies, our GaN PD (1:20), which was fabricated through a very cost-effective production method, exhibited excellent performance in terms of both responsivity (8.51 A/W under 302 nm) and detectivity (1.82×10^{13} Jones under 302 nm).

4 Conclusion

In this work, the effect of Au electrode asymmetry on the GaN photodetector performance was systematically investigated through the electrodes area ratio ranging from 1:2 to 1:20. With increasing Au electrode asymmetry, the device performance was substantially enhanced under both 302 nm and 365 nm UV illumination at zero bias. The GaN photodetector achieved its best performance, with a responsivity of 8.51 A/W and a specific detectivity of 2.42×10^{13} Jones, using a 1:20 asymmetrical Au electrode ratio under 302 nm illumination. This enhancement in photoresponsivity is attributed to the increased Au electrode size asymmetry due to the built-in potential difference caused by the non-uniform lowering of Schottky barriers at the Au/GaN junctions under illumination. Consequently, the combination of a cost-effective fabrication process and simple processing steps delivers excellent device performance, demonstrating strong potential for high-performance self-powered sustainable photodetection applications.

Acknowledgements The authors gratefully thank the Boğaziçi University Research Fund for providing support for this research (Project No: 20403).

Authors contribution Sahan Tetik performed the experiments, analyzed the data, and wrote the manuscript. Kasif Teker designed the experiment, supervised the project, wrote the manuscript, provided resources, and revised the manuscript.

Funding Open access funding provided by the Scientific and Technological Research Council of Türkiye (TÜBİTAK).

Data availability The data is available upon reasonable request.

Declarations

Conflict of interest The authors declare no competing interests.

Open Access This article is licensed under a Creative Commons Attribution 4.0 International License, which permits use, sharing, adaptation, distribution and reproduction in any medium or format, as long as you give appropriate credit to the original author(s) and the source, provide a link to the Creative Commons licence, and indicate if changes were made. The images or other third party material in this article are included in the article's Creative Commons licence, unless indicated otherwise in a credit line to the material. If material is not included in the article's Creative Commons licence and your intended use is not permitted by statutory regulation or exceeds the permitted use, you will need to obtain permission directly from the copyright holder. To view a copy of this licence, visit http://creativecommons.org/licenses/by/4.0/.

References

1. Y. Wang, S. Li, Y. Huang et al., Photomultiplication-type organic photodetectors: mechanisms, integration toward next-generation sensing platforms. Adv. Funct. Mater. **n/a**, e18958 (2025). https://doi.org/10.1002/adfm.202518958
2. Y. Li, X. He, S.-C. Chen, N. Zhao, Intelligent photodetectors: post manufacturing tunability toward enhanced performance and advanced functions. Chem. Rev. **125**, 6977–7022 (2025). https://doi.org/10.1021/acs.chemrev.4c00763
3. V. Laxmi, Y. Tu, D. Tyagi et al., Recent progress in ultraviolet photodetectors based on low-dimensional materials. Nanoscale **17**, 11246–11274 (2025). https://doi.org/10.1039/D4NR04317K
4. Z. Bi, X. Liu, Z. Liu et al., Sol-gel synthesized UV photodetector with low dark current based on $MgZnO/Nb_2O_5$ heterojunction. Mater. Sci. Semicond. Process. **202**, 110174 (2026). https://doi.org/10.1016/j.mssp.2025.110174
5. G. Li, B. Cheng, H. Zhang et al., Progress in UV photodetectors based on ZnO nanomaterials: a review of the detection mechanisms and their improvement. Nanomaterials (2025). https://doi.org/10.3390/nano15090644
6. L. Ge, M. Wang, X. Chen et al., High-performance p-Te/n-SiC heterojunction for self-powered UV photodetection and imaging. IEEE Electron Device Lett. **47**, 49–52 (2026). https://doi.org/10.1109/LED.2025.3625655
7. S. Sakalley, A. Saravanan, W.-C. Cheng et al., High performance self-powered UV photodetection by ZnO/Cu_3N core-shell nanorod heterostructures via p-n junction formation. J. Alloys Compd. **936**, 168157 (2023). https://doi.org/10.1016/j.jallcom.2022.168157
8. J. Wang, Y. Xing, F. Wan et al., Progress in ultraviolet photodetectors based on II–VI group compound semiconductors. J. Mater. Chem. C **10**, 12929–12946 (2022). https://doi.org/10.1039/D2TC02127G
9. Vashishtha P, Goswami L, Jain SK, et al (2023) GaN-Djoser Pyramidal Self Powered UV Photodetector for Optical Signal Detection in Rugged Environments. J Alloys Compd 930:167267. https://doi.org/10.1016/j.jallcom.2022.167267
10. T.U. Teker, K. Teker, Enhanced photoresponse of a self-powered gallium nitride photodetector via sequentially-deposited gold nanoparticles for sustainable optoelectronics. J. Electron. Mater. **52**, 2372–2379 (2023). https://doi.org/10.1007/s11664-022-10176-x
11. K. Teker, S. Tetik, Enhanced photoresponse of a gold nanoparticle-modified single SiC nanowire UV photosensor. Sens. Actuators A Phys. **396**, 117227 (2025). https://doi.org/10.1016/j.sna.2025.117227 10.1016/j.sna.2025.117227
12. Zoysa Y De, Saminda D, Thalayarathna C, et al (2025) Tailoring ZNO Nanostructure for Enhanced Capacitive UV Response. In: 2025 Moratuwa Engineering Research Conference (MERCon). pp 788–793
13. L. Yang, H. Zhang, Y. Sun et al., Temperature-dependent photodetection behavior of AlGaN/GaN-based ultraviolet phototransistors. Appl. Phys. Lett. **120**, 091103 (2022). https://doi.org/10.1063/5.0083171
14. Gu Y-J, Li S, Wang Y-X, et al (2025) Solar-Blind UV Photodetector Based on Anisotropic Ga_2O_3/MgO Heteroepitaxial Structure for Polarization Imaging. IEEE Trans Electron Devices 1–6. https://doi.org/10.1109/TED.2025.3648696
15. K. Teker, Aluminium nitride nanowire array films for nanomanufacturing applications. Mater. Sci. Technol. **31**, 1832–1836 (2015). https://doi.org/10.1179/1743284715Y.0000000027
16. L. Ge, Y. Peng, B. Li et al., A highly responsive hydrogen-terminated diamond-based phototransistor. IEEE Electron Device Lett. **43**, 1271–1274 (2022). https://doi.org/10.1109/LED.2022.3180845
17. Y. Liu, B.E. Kruschwitz, M.J. Bonino et al., Effect of illumination area on the ultrafast temporal response of MSM GaN photodiodes. IEEE Trans. Electron Devices **73**, 894–899 (2026). https://doi.org/10.1109/TED.2025.3647826
18. K. Teker, S. Tetik, Plasmonic enhancement of UV detection in Au nanoparticle-decorated SiC nanowire phototransistors. Appl. Surf. Sci. **728**, 166194 (2026). https://doi.org/10.1016/j.apsusc.2026.166194
19. Gong B, Ge M, Wang X, et al (2024) AlGaN/GaN HEMT-Based MHM Ultraviolet Phototransistor With Bent-Gate Structure. IEEE Electron Device Letters 45:2335–2338. https://doi.org/10.1109/LED.2024.3483730
20. Wang J, Ma S, Zhang S, et al (2026) High Detection Rate Self-Powered Ultraviolet Photodetector Based on the Mixed-dimensional BP/n-GaN Heterojunction. IEEE Journal of Selected Topics in Quantum Electronics 1–9. https://doi.org/10.1109/JSTQE.2026.3672974
21. Nguyen TMH, Shin SG, Choi HW, Bark CW (2022) Recent advances in self-powered and flexible UVC photodetectors. Exploration 2:20210078. https://doi.org/10.1002/EXP.20210078
22. Wu T-Y, Wang L-W, Chen B-C, et al (2024) Investigations of MoS_2-Based Self-Powered M–S–M Photodetectors with Low Defect Density and Fast Response and Low-Temperature Characteristics. ACS Appl Electron Mater 6:702–711. https://doi.org/10.1021/acsaelm.3c01123
23. Freeouf JL, Jackson TN, Laux SE, Woodall JM (1982) Effective barrier heights of mixed phase contacts: Size effects. Appl Phys Lett 40:634–636. https://doi.org/10.1063/1.93171
24. Aggarwal N, Krishna S, Sharma A, et al (2017) A Highly Responsive Self-Driven UV Photodetector Using GaN Nanoflowers. Adv Electron Mater 3:1700036. https://doi.org/10.1002/aelm.201700036
25. Chen H-Y, Liu K-W, Chen X, et al (2014) Realization of a self-powered ZnO MSM UV photodetector with high responsivity using an asymmetric pair of Au electrodes. J Mater Chem C Mater 2:9689–9694. https://doi.org/10.1039/C4TC01839G
26. Gu K, Zhang Z, Huang H, et al (2023) Tailoring photodetection performance of self-powered Ga_2O_3 UV solar-blind photodetectors through asymmetric electrodes. J Mater Chem C Mater 11:5371–5377. https://doi.org/10.1039/D3TC00387F
27. Zhou C, Raju S, Li B, et al (2018) Self-Driven Metal–Semiconductor–Metal WSe_2 Photodetector with Asymmetric Contact Geometries. Adv Funct Mater 28:1802954. https://doi.org/10.1002/adfm.201802954
28. J. Huang, L. Yang, S. He, High-performance low-voltage transparent metal-semiconductor-metal ultraviolet photodetectors based on ultrathin gold asymmetric interdigitated electrodes. Micromachines **14**, 14071447 (2023). https://doi.org/10.3390/mi14071447
29. B. Singh, V. Aggarwal, R. Kumar et al., Tailoring GaN nanorods with MoS_2 on tungsten foil for enhanced photoelectrochemical performance. Front. Energy **19**, 767–778 (2025). https://doi.org/10.1007/s11708-025-1035-z
30. Y. Hou, Z. Mei, X. Du, Semiconductor ultraviolet photodetectors based on ZnO and MgxZn1−xO. J. Phys. D Appl. Phys. **47**, 283001 (2014). https://doi.org/10.1088/0022-3727/47/28/283001
31. N.K.R. Nallabala, V.R.M. Reddy, V.R. Singh et al., Enhanced photoresponse performance in GaN based symmetric type MSM ultraviolet-A and MIS ultraviolet-A to C photodetectors. Sens. Actuators A Phys. **339**, 113502 (2022). https://doi.org/10.1016/j.sna.2022.113502
32. D. Guo, Z. Wu, P. Li et al., Opt. Mater. Express **4**, 1067–1076 (2014). https://doi.org/10.1364/OME.4.001067
33. P. Vashishtha, P. Prajapat, A. Sharma et al., Self-driven UVC–NIR broadband photodetector with high-temperature reliability based on a coco palm-like MoS2/GaN heterostructure. ACS Appl.

Electron. Mater. **5**, 1891–1902 (2023). https://doi.org/10.1021/acsaelm.3c00156
34. H. Tian, C. Fan, G. Liu et al., Ultrafast broadband photodetector based on SnS synthesized by hydrothermal method. Appl. Surf. Sci. **487**, 1043–1048 (2019). https://doi.org/10.1016/j.apsusc.2019.05.175
35. V.K. Pulikodan, A.M. Raees, A. Alexander et al., Origin of anomalous transient photocurrent in solution-processed WS2 nanosheet-based self-powered photodetectors. ACS Appl. Nano Mater. **7**, 8007–8021 (2024). https://doi.org/10.1021/acsanm.4c00590
36. E. Monroy, F. Omnès, F. Calle, Wide-bandgap semiconductor ultraviolet photodetectors. Semicond. Sci. Technol. **18**, R33 (2003). https://doi.org/10.1088/0268-1242/18/4/201
37. U. Varshney, A. Sharma, L. Goswami et al., Deep ultraviolet–visible highly responsivity self-powered photodetector based on β-Ga_2O_3/GaN heterostructure. Vacuum **217**, 112570 (2023). https://doi.org/10.1016/j.vacuum.2023.112570
38. T. Chen, X. Zhang, Y. Ma et al., Self-powered and spectrally distinctive nanoporous Ga_2O_3/GaN epitaxial heterojunction UV photodetectors. Adv. Photonics Res. **2**, 2100049 (2021). https://doi.org/10.1002/adpr.202100049
39. J. Dong, D. Zhang, Y. Ma et al., Plasmon-enhanced self-powered GaN/ZnTe core/shell nanopillar array photodetector. Nano. Res. **17**, 5569–5577 (2024). https://doi.org/10.1007/s12274-024-6477-9
40. P. Li, H. Shi, K. Chen et al., Construction of GaN/Ga_2O_3 p–n junction for an extremely high responsivity self-powered UV photodetector. J. Mater. Chem. C **5**, 10562–10570 (2017). https://doi.org/10.1039/C7TC03746E
41. H. Liu, P. Wan, M. Chen et al., Integrating interface engineering and plasmonic effect to boost photoresponse performance of ZnO:Ga/GaN heterojunction self-powered UV photodetectors. J. Lumin. **269**, 120518 (2024). https://doi.org/10.1016/j.jlumin.2024.120518
42. X. Lin, H. Deng, Y. Jia et al., Self-powered Sb_2S_3 thin-film photodetectors with high detectivity for weak light signal detection. ACS Appl. Mater. Interfaces **14**, 12385–12394 (2022). https://doi.org/10.1021/acsami.1c25256
43. M.A. Yildirim, K. Teker, Self-powered silicon carbide ultraviolet photodetector via gold nanoparticle plasmons for sustainable optoelectronic applications. Phys. Scr. **97**, 115804 (2022). https://doi.org/10.1088/1402-4896/ac9562

Publisher's note Springer Nature remains neutral with regard to jurisdictional claims in published maps and institutional affiliations.